Turkish Journal of Physics

http://journals.tubitak.gov.tr/physics/

Research Article

Turk J Phys
(2019) 43: 516 – 530

doi:10.3906/fiz-1906-6

CCD $UBVRI$ photometry of the open cluster Berkeley 8

Hikmet ÇAKMAK[1*], Raúl MICHEL[2], Yüksel KARATAŞ[1]

[1]Department of Astronomy and Space Sciences, Faculty of Science, İstanbul University, 34116, İstanbul, Turkey
[2]National Astronomical Observatory, National Autonomous University of Mexico, Ensenada, Baja California, Mexico

Received: 11.06.2019 • **Accepted/Published Online:** 07.08.2019 • **Final Version:** 21.10.2019

Abstract: The poorly studied Berkeley 8 (Be 8) open cluster is analyzed from CCD $UBVRI$ photometric data taken with the 0.90 m telescope at the Sierra Nevada Observatory. The $Z = +0.008$ PARSEC isochrone gave us a reddening of E(B-V) = 0.69 ± 0.03, a distance of 3410 ± 300 pc, and an age of 2.8 ± 0.2 Gyr. Its median Gaia DR2 distance, d = 3676 ± 810 pc, is in good agreement with our photometric distances, 3410–3620 pc within the uncertainties. The kinematic parameters of five likely members of Be 8 with the circular orbits, ecc = [0.23, 0.30], reflect the properties of the Galactic thin disc, which is also consistent with what is expected of its metal content ([M/H] = –0.27). Be 8 with R > 9 kpc (co-rotation gap at 9 kpc) may have been originating from a different galactic radius or different star formation region.

Key words: Galaxy, open clusters and associations, abundances, evolution

1. Introduction

Open clusters (OCs) are valuable objects for revealing stellar evolution and the structure, chemical, and dynamical evolution of the Galactic disc. Berkeley 8 (Be 8) was studied by Hasegawa et al. [1] from CCD BVI photometry and by Bukowiecki et al. [2] from 2MASS JHK$_s$ photometry. Be 8 is located close to a portion of the Perseus spiral arm in the second quadrant of the Galaxy (Figure 1), according to its equatorial and Galactic coordinates (WEBDA) [3] (rows 1–4 of Table 1). The main aim of this paper is to present astrophysical parameters such as reddening, distance, and age of Be 8 from four color indices, $(B-V)$, $(V-I)$, $(R-I)$, and $(G_{BP}–G_{RP})$, obtained from deep CCD $UBVRI$ and Gaia photometries. This kind of data is also valuable for classifying early-type stars, Blue Stragglers (BS), and Red Giant/Red Clump (RG/RC) candidates in the color magnitude diagrams (CMDs), and thus probable candidates are proposed for future spectroscopic observations. We used Gaia DR2 astrometric data (proper motion components and parallaxes) [4, 5] and Gaia DR2 photometry (G - G$_{BP}$G$_{RP}$) for determining the probable members of Be 8. With the Gaia DR2 astrometric data, a membership method was applied in the literature [6–8]. The membership determinations of previous works have been based on the proper motions of Roeser et al. [9] in combination with the 2MASS JHK$_s$ photometry of Skrutskie et al. [10]. Cantat-Gaudin et al. [11] stated that the proper motion uncertainties of UCAC4 fall in the range of 1–10 mas yr^{-1} [9, 12]. According to Lindegren et al. [4] and Brown et al. [5], the mean parallax errors of the Gaia DR2 catalogue fall in the range of 0.02–0.04 mas for G < 15 and 0.1 mas for G < 17, whereas the uncertainties of proper motion components are up to 0.06 mas yr^{-1} for G < 15 mag

*Correspondence: hcakmak@istanbul.edu.tr

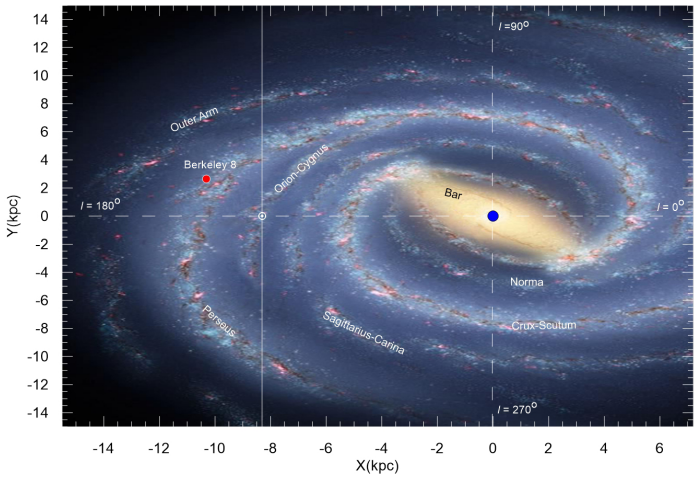

Figure 1. Spatial distribution (X, Y) (kpc) (filled red circle) of Be 8. See Section 6 for the estimation of (X, Y) values. The sun is at $R_{\odot}$ = 8.2 ± 0.1 kpc [34]. The image is adapted from the image[1] by Robert Hurt, IPAC; Bill Saxton, NRAO/AUI/NSF.

Table 1. Rows 1–4 provide the central equatorial (J2000) and the Galactic coordinates of WEBDA. Air mass and exposure times (s) of filters are listed in rows 5–10.

Cluster	Be 8
α_{2000} (h m s)	02 01 08.00
δ_{2000} (° ′ ″)	+75 29 38.25
ℓ (°)	127.35
b (°)	+13.21
Air mass	1.276 – 1.280
Filter U Exp.Time (s)	9, 90, 3×300
Filter B Exp.Time (s)	5, 50, 500
Filter V Exp.Time (s)	3, 30, 300
Filter R Exp.Time (s)	2, 20, 200
Filter I Exp.Time (s)	2, 20, 200

and 0.2 mas yr^{-1} for G < 17.

This paper is organized as follows: Section 2 describes the observation and reduction techniques. Its dimensions are given in Section 3. Section 4 is devoted to the classification of cluster members. Section 5 describes the derivation of the astrophysical parameters. The classification of BS and RG/RC candidates and morphological age determination are presented in Section 6. Section 7 focuses on its kinematics and orbital parameters. Discussion and conclusions are given in Section 8.

2. Observations and reduction techniques

Observations of Be 8 were carried out during the photometric night of December 3, 2015, with the 0.90 m (f/8 Ritchey-Chrétien) telescope at the Sierra Nevada Observatory (Granada, Spain). A filter wheel with $UBVRI$ filters and a scientific grade Marconi-EEV CCD42-40 were employed. The CCD is a 2048×2048 13.5 μm

[1] https://www.universetoday.com/102616/our-place-in-the-galactic-neighborhood-just-got-an-upgrade

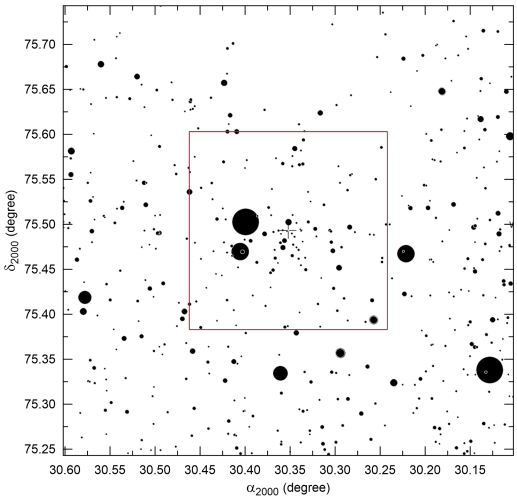

Figure 2. The image of Be 8 for a region of $18.3' \times 17.2'$ (https://www.aavso.org (AAVSO)). The red rectangle indicates the field of view of the SNO detector, $13.2' \times 13.2'$.

square-pixel detector with a nominal gain of 1.35 e^-/ADU and a readout noise of 7.14 e^- with 2×2 binning employed. Along with the optics, it covers a field of view of 13.2×13.2 arcmin^2. Apart from Be 8, other open clusters and some Landolt standard fields [13] were observed. Flat fields were also acquired at the beginning of the night and many bias frames were also taken.

The data reduction was carried out by R. Michel [2] using the IRAF[3] package together with some home-made auxiliary Fortran programs and Awk scripts. All the images were bias subtracted and flat-field corrected (CCDRED). Cosmic rays were removed with the L.A. Cosmic[4] script van Dokkum [14].

The standard magnitudes were taken from the catalogue by Landolt [13] and supplemented with the secondary photometric standards by Cutri et al. [15]. As a result, the transformation coefficients were found (FITPARAMS). For magnitude estimation, the transformation equations used are

$$M_\lambda = m_\lambda - (k_1 - k_2 C)X + \eta_\lambda C + \zeta_\lambda, \tag{1}$$

where m_λ, k_1, k_2, C, and X are observed instrumental magnitude, primary and secondary extinction coefficients, color index, and air mass, respectively. M_λ, η_λ, and ζ_λ are standard magnitude, atmospheric extinction-corrected instrumental magnitude, transformation coefficient, and photometric zero point, respectively. The other details of data reduction can be found in the papers of Akkaya et al. [16, 17]. Air-mass range and exposure times in each band during the observations are given in rows 5–10 of Table 1.

Figure 2 presents the finding chart[5] of Be 8 ($18.3' \times 17.2'$). The red rectangle indicates the field of view of the SNO detector, $13.2' \times 13.2'$. The photometric errors in V and $(R-I)$, $(V-I)$, $(B-V)$, $(U-B)$ of Be 8 are presented in Figure 3. Its mean photometric errors are also listed in Table 2. Our inspection of Figure

[2]Data may be requested from R. Michel.
[3]IRAF is distributed by the National Optical Observatories, operated by the Association of Universities for Research in Astronomy, Inc., under cooperative agreement with the National Science Foundation.
[4]http://www.astro.yale.edu/dokkum/lacosmic
[5]Obtained from https://www.aavso.org (AAVSO) [accessed 09 June 2019].

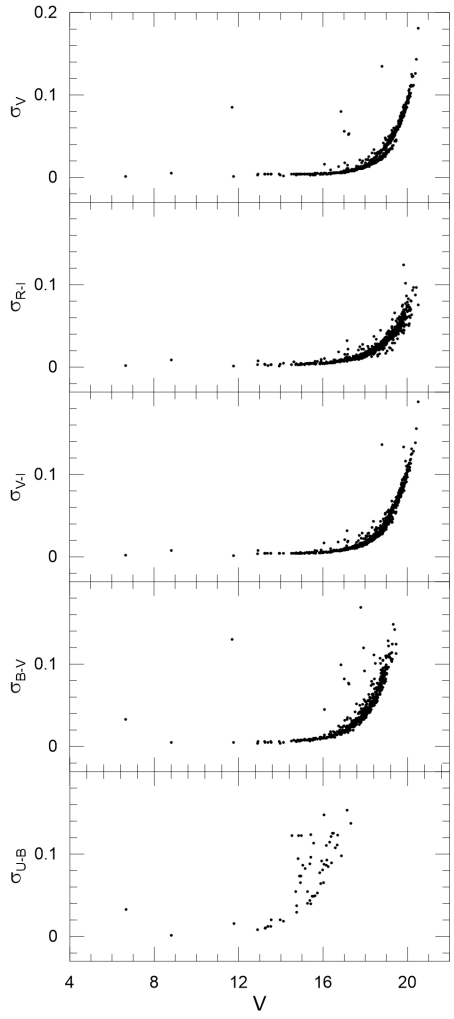

Figure 3. Photometric errors of the V apparent magnitude and four colors against the V magnitude for Be 8.

Table 2. The mean photometric errors of V, $(U-B)$, $(B-V)$, $(R-I)$, and $(V-I)$ of Be 8.

V	σ_V	σ_{U-B}	σ_{B-V}	σ_{R-I}	σ_{V-I}	N
6 - 13	0.017	0.014	0.031	0.004	0.004	6
13 - 14	0.004	0.014	0.005	0.003	0.004	7
14 - 15	0.004	0.074	0.007	0.004	0.004	13
15 - 16	0.004	0.071	0.009	0.005	0.005	30
16 - 17	0.007	0.104	0.018	0.007	0.009	50
17 - 18	0.011	0.145	0.034	0.012	0.015	166
18 - 19	0.022	-	0.063	0.023	0.027	265
19 - 20	0.058	-	0.110	0.047	0.066	216
20 - 21	0.107	-	-	0.073	0.117	30

3 and Table 2 indicates that stars brighter than $V = 18$ have errors smaller than 0.03 in $(R-I)$, $(V-I)$, $(B-V)$. For $V > 20$, the errors in $(R-I)$ and $(V-I)$ are larger than 0.03. After $V > 18$, the errors in $(B-V)$ are up to $\approx 0^m.03$. The errors in $(U-B)$ are less than 0.01 for $V < 14$, whereas for $14 < V \leq 18$, large errors increase.

3. Dimensions of Be 8

The stellar radial density profile (RDP) of Be 8 (Figure 4) has been built from Gaia DR2 photometry for the equatorial coordinates (Table 1). Its RDP has been constructed by counting stars in concentric rings of increasing width with distance to its center. We choose $\Delta R = 15.0'$ as the wide external ring of the stellar comparison field. As emphasized by Bonatto and Bica [18], the number and width of rings were optimized so that the resulting RDP had adequate spatial resolution with moderate 1σ Poisson errors. The solid curve (Figure 4) denotes the fitted King's profile [19]. Here we adopt the two-parameter function, $\sigma(R) = \sigma_{bg} + \sigma_0/(1+(R/R_c)^2)$, where σ_{bg} is the residual background density, σ_0 the central density of stars, and R_{core} the core radius. The horizontal red bar shows the stellar background level measured in the comparison field, and the 1σ profile fit uncertainty is shown by the shaded region. The core and cluster radii from Figure 4 have been determined as $R_{core} = 1.8'$ and $R_{RDP} = 15.0'$, respectively. These dimensions are quite close to the ones of $(R_{core},\ R_{RDP}) = (1.52',\ 15.5')$ of Bukowiecki et al. [2].

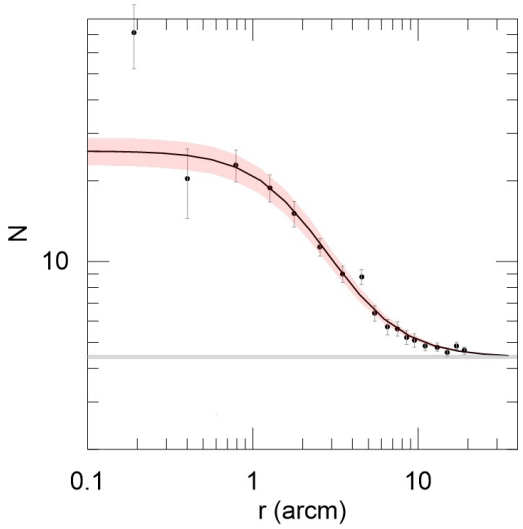

Figure 4. Stellar RDP (filled dots) of Be 8. Solid line shows the best-fit King profile. Horizontal red bar: stellar background level measured in the comparison field. Shaded region: 1σ King fit uncertainty. The core and cluster radii are obtained as $R_{core} = 1.8'$ and $R_{RDP} = 15.0'$, respectively.

4. Classification of cluster members

For the membership determination of Be 8, our CCD $UBVRI$ photometric data have been matched with Gaia DR2 astrometric (proper motion components and parallaxes) (μ_α, μ_δ, and ϖ) and Gaia DR2 photometric data. μ_α versus μ_δ $(mas\ yr^{-1})$ for all stars of Be 8 (filled dots) is shown in Figure 5. Gray dots denote the

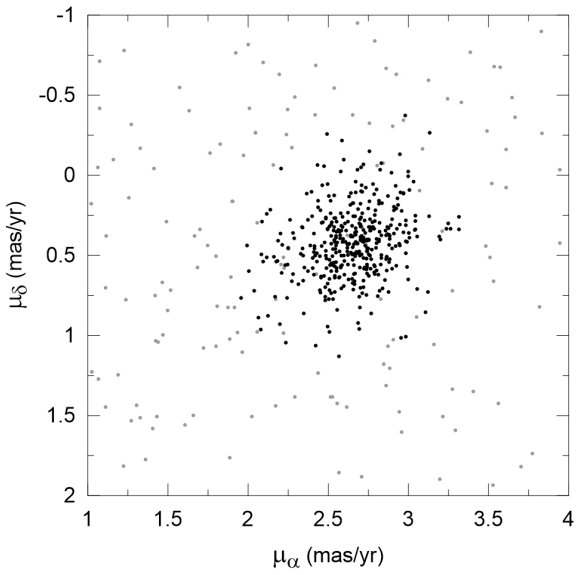

Figure 5. μ_α versus μ_δ for Be 8 (filled stars). Small gray dots represent the Gaia DR2 astrometric data for a $15'.0$ field centered on Be 8.

field stars inside $R = 15'.0$ arcmin centered on Be 8. We have applied the Gaussian mixture method for all stars of Be 8.

By applying the Gaussian Mixture Model (GMM) [20] to the stars in the cluster region of Be 8, we have determined the membership probability (P). The model considers that the distribution of proper motions of the stars in a cluster's region can be represented by two elliptical bivariate Gaussians, by following Wu et al. [21], which include the proper motion's errors in the frequency function. The expressions used can be found in the papers of Balaquer-Nunez et al. [6], Sariya et al. [7], and Dias et al. [8]. P is defined as Φ_c /Φ. Here $\Phi = \Phi_c + \Phi_f$ is the total probability distribution. c and f subscripts are for cluster and field parameters, respectively. The used parameters for estimation of Φ_c and Φ_f are μ_α, μ_δ, ϖ, $\sigma_{\mu\alpha}$, $\sigma_{\mu\delta}$, and σ_ϖ. The averages and their uncertainties of proper motion components and parallaxes in the distributions of the cluster and field regions in Figure 5 are listed in Table 3. Figure 6a shows the membership probability (P) histogram, which provides a very clear separation between cluster and field stars. The number of stars with membership probability greater than 90% is 273. These likely members have been considered for deriving astrophysical parameters of Be 8. From the relation of the membership probability (P) versus G mag (Figure 6b), high membership probability appears to extend down to G $\sim$ 21 mag.

Table 3. The medians and their uncertainties of proper motion components (μ_α, μ_δ) ($mas\ yr^{-1}$) and parallaxes (ϖ) (mas) from the distributions of the cluster and field regions in Figure 5.

	$\mu_\alpha \pm \sigma_{\mu\alpha}$	$\mu_\delta \pm \sigma_{\mu\delta}$	$\varpi \pm \sigma_\varpi$
Cluster region	2.648 ± 0.24	0.421 ± 0.23	0.266 ± 0.12
Field region	0.33 ± 2.23	0.347 ± 1.75	0.545 ± 0.45

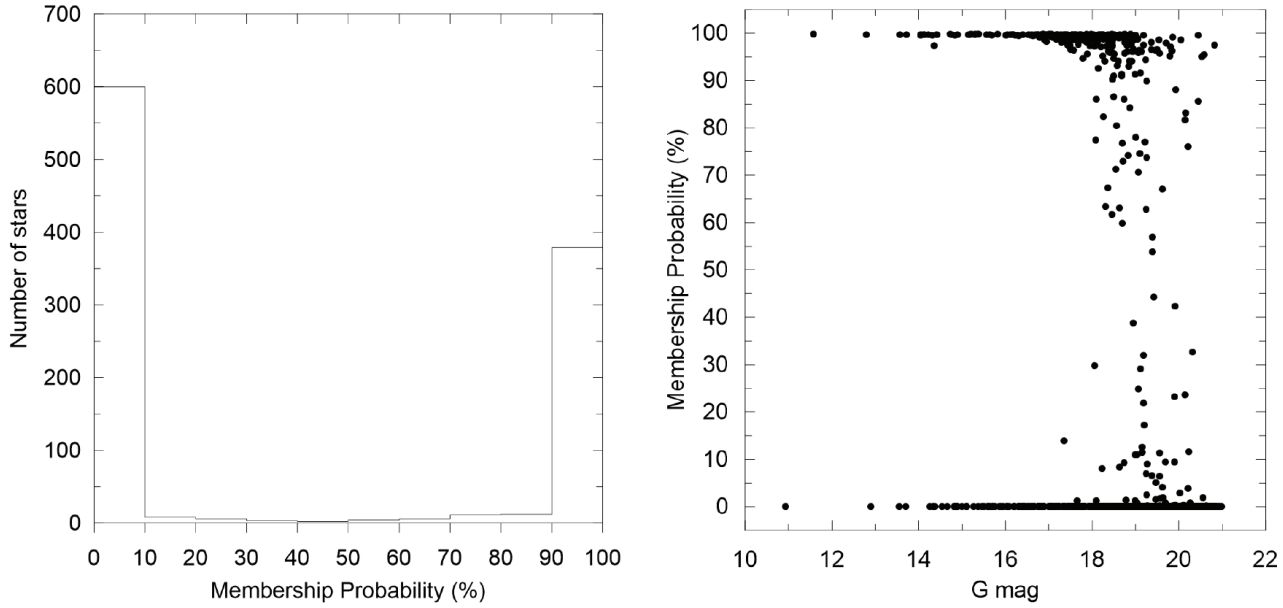

Figure 6. Membership probability histogram P(%) (left panel) and P(%) versus G mag (right panel) for all stars of Be 8.

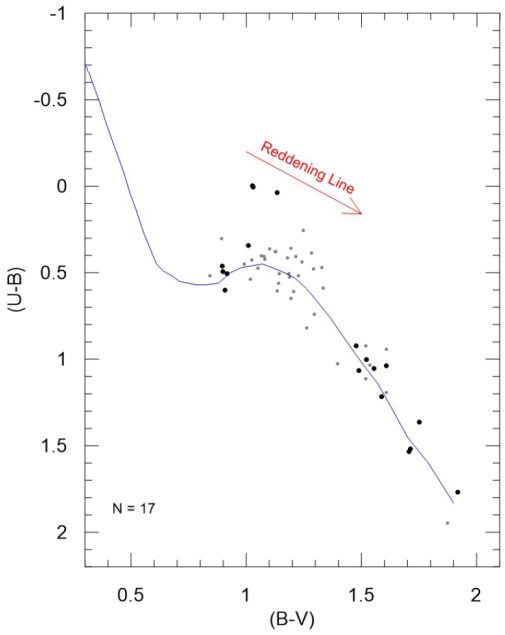

Figure 7. $(U-B)$ - $(B-V)$ two-color diagram for the 17 likely members (filled dots) of Be 8. The dashed blue line represents the Schmidt-Kaler (SK82) main sequence. Field stars are shown with small gray dots. Red arrow denotes the reddening.

Table 4. The derived fundamental astrophysical parameters of Be 8 for four color indices.

Color	$(V_0–M_V)$	d (kpc)	log (A)	A (Gyr)
$(B-V)$	12.66 ± 0.19	3.41 ± 0.30	9.45 ± 0.03	2.80 ± 0.20
$(V-I)$	12.67 ± 0.31	3.42 ± 0.49	9.45 ± 0.03	2.80 ± 0.20
$(R-I)$	12.79 ± 0.32	3.62 ± 0.53	9.45 ± 0.03	2.80 ± 0.20
$(G_{BP}-G_{RP})$	12.71 ± 0.31	3.48 ± 0.50	9.45 ± 0.03	2.80 ± 0.20

5. Astrophysical parameters of Be 8 open cluster

The two-color $(U-B)$ - $(B-V)$ (CC) diagram of the 17 probable members for Be 8 is displayed in Figure 7. The blue line denotes the reddened main sequence for dwarfs and red giants of Schmidt-Kaler (SK82) [22]. It appears from Figure 7 that Be 8 contains F-type stars, which are quite valuable for determining photometric metal abundance, [M/H]. These F-type stars with $(U-B) < 0.35$ and $0.9 < (B-V) < 1.2$ have large UV excesses, $\delta(U-B)$ =0.15–0.48. A member star with $\delta(U-B) = 0.15$ estimates $[M/H] = -1.0$, which is very poor for Galactic open clusters. The other three members with $\delta(U-B)$ =0.47–0.48 do not allow us determine a reasonable [M/H] value due to their large UV excesses, which are insensitive to the metal abundance calibration (see the paper of Karataş and Schuster [23]). Moreover, their photometric errors in $(U-B)$ are larger at a level of $\sigma_{(U-B)}$ =0.10–0.15.

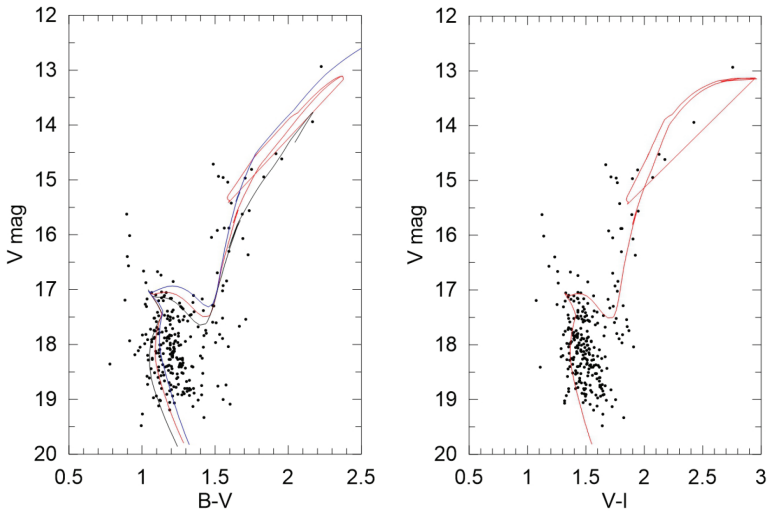

Figure 8. For the 268 likely members of Be 8, CMDs of V - $(B-V)$ (left) and V - $(V-I)$ (right). Red curves show the PARSEC isochrones interpolated to $Z = +0.008$. In the left figure, the fitted isochrones $Z = +0.015$ (blue line) and +0.004 (black line) are also plotted (see Section 5).

Since these issues make it difficult to determine the photometric metal abundance and reddening from the CC diagram, we have derived the reddenings, distance moduli, and ages of Be 8 from the PARSEC isochrones of Bressan et al. [24] on the CMDs for four color indices. The appropriate PARSEC isochrones for different heavy element abundance mass fractions (Z = +0.015, +0.004, +0.008) (left panel of Figure 8) and reddenings

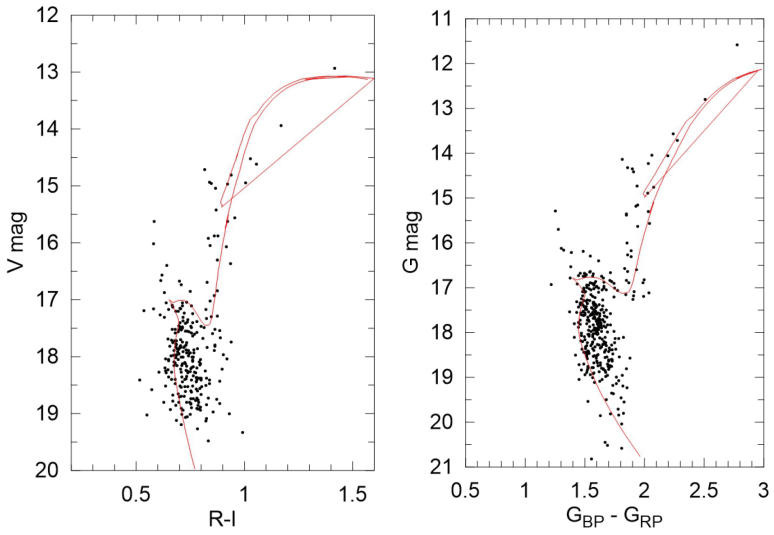

Figure 9. For the 268 likely members of Be 8, CMDs of V - $(R-I)$ (left) and G - $(G_{BP}-G_{RP})$ (right). The meanings of the symbols are the same as in Figure 8.

have been fitted on the CMDs. The 2.8 Gyr PARSEC isochrones for Z = +0.008 abundance gave us a good fit solution on the CMDs: V - $(B-V)$, V - $(V-I)$, V - $(R-I)$, G - $(G_{BP}-G_{RP})$ (Figures 8 and 9). The equation $Z = Z_{\odot}10^{[M/H]}$ estimates its photometric metal abundance as [M/H] $= -0.27$. Here the solar heavy metal content is adopted as $Z_{\odot} = +0.015$. The isochrone is varied until a satisfactory fit to the data has been obtained through the observed main-sequence (MS), turn-off (TO), sub-giant (SG), and Red Giant/Red Clump (RG/RC) sequences on the CMDs, as we followed the papers of Akkaya et al. [16, 17] and Güneş et al. [25]. Because of the presence of binaries, the PARSEC isochrones have been shifted to the left and below the MS on all CMDs. The vertical shift gives the (true) distance modulus, $DM = (V_0 - M_{\rm V})$. For its age (A, log(A)), the PARSEC isochrones have been shifted both vertically and horizontally on the CMDs with the expression $M_V + 3.1E(B-V) + DM$ for the vertical displacement and $C_0(\lambda_1-\lambda_2) + E(\lambda_1-\lambda_2)$ for the horizontal, where λ denotes the wavelengths of $BVRI$ and G, G_{BP}, G_{RP} filters. Here C_0 means the dereddened color index. The obtained reddenings from four CMDs are E(B−V) = 0.69 ± 0.08, E(V−I) = 0.87 ± 0.10, E(R−I) = 0.44 ± 0.05, and E($G_{BP}-G_{RP}$) = 0.91 ± 0.10, respectively. Its distance moduli (V_0 – $M_{\rm V}$)/ distances (d (kpc)) and age (Gyr) for four colors are presented in columns 2–5 of Table 4. In order to deredden the distance moduli (column 2 of Table 4) for the color indices $(V-I)$, $(R-I)$, and $(G_{BP}-G_{RP})$, our color excesses E(V − I), E(R−I), and E($G_{BP}-G_{RP}$) have been converted from the relations E(V − I) = 1.25 E(B−V), E(R−I) = 0.69 E(B−V) [26–28], and E(B−V) = 0.775 E($G_{BP}-G_{RP}$) [29].

6. Blue Stragglers, Red Giants/Clumps, and morphological age index

>From Figures 8 and 9 we note that six probable Blue Straggler (BS) candidates lie on $(B-V) < 1.1$, $(V-I) < 1.4$, $(R-I) < 0.7$ for $V < 17.0$, whereas they occupy the region with $G < 16.75$ and G_{BP} - $G_{RP} < 1.4$. BS candidates blur the main-sequence turn-off (TO) to a brighter magnitude. RG/RC candidates populate the red-giant branch well (Figures 8 and 9). These RG/RC stars in old clusters are numerous and

luminous as expected. BS (blue plus symbol) and RG/RC (red plus) candidates with P > 90% have been placed on the nested circles of Figure 10. Two BS candidates reside in the core radius of 1.8 ′ of Be 8. Four BS stars occupy the inner regions. Twenty-six RG/RC candidates remain within the cluster radius ($R_{RDP} = 15.0'$). Their median Gaia DR2 distances are d = 3953 ± 750 pc (ϖ = 0.253 ± 0.048 mas) (six BS) and d = 4049 ± 610 pc (ϖ = 0.247 ± 0.037 mas) (26 RG/RC), respectively, which are in reasonable agreement with the photometric ones within the uncertainties (Table 4). However, spectroscopic observations of these candidates are needed for their membership confirmation.

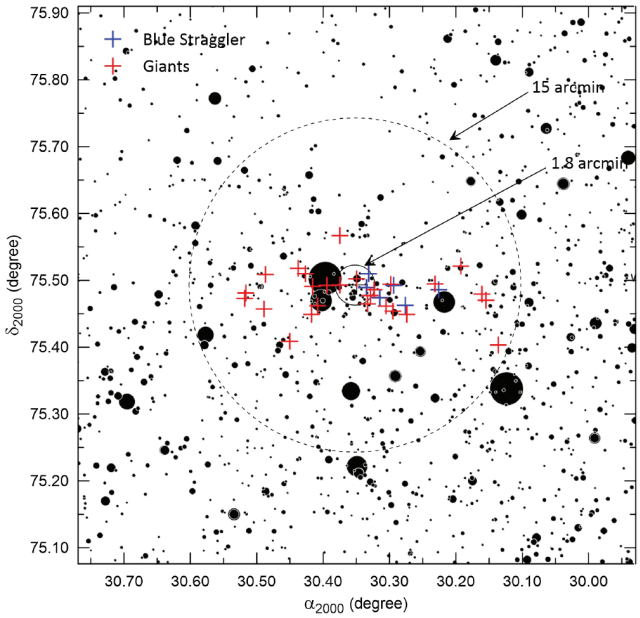

Figure 10. Circles have been drawn for the radii of 1.8′ and 15.0′ arc min on the α_{2000} versus δ_{2000} of Be 8. Red and blue pluses represent the RG/RC and BS candidates on the CMDs (Figures 8 and 9).

The CMDs of Be 8 exhibit noticeable TO and RG/RC sequences (Figures 8 and 9). By utilizing the definition of the morphological age index (MAI), $\delta 1 = (B - V)_{TO} - (B - V)_{RG}$ given by Phelps et al. [30], we measured V_{TO} = 17.07, $(B-V)_{TO}$ = 1.066, and $(B-V)_{RG}$ = 1.599 on the V - $(B-V)$ diagram (left panel of Figure 8). These values estimate $\delta 1$ = 0.533. Here $\delta 1$ is the difference in the color indices between the bluest point of TO and the color at the base of the RG branch one magnitude brighter than the TO luminosity. Our $\delta 1$ value has been transformed into δV via the equation of $\delta V = 3.77 - 3.75\delta 1$ of Phelps et al. [30]. Its morphological age has been estimated as log A = 9.45 (A = 2.94 Gyr) from the equation $logA = 0.04\delta V^2 + 0.34\delta V + 0.07[Fe/H] + 8.76$ of Salaris et al. [31], applying its metal abundance ([M/H] = −0.27) and δV = 1.771. Here we assume [Fe/H] ≈ [M/H]. Its MAI age (2.94 Gyr) is compatible with its isochrone age, 2.80 Gyr.

7. Kinematics and orbital parameters of Be 8

Five likely members with Gaia DR2 radial velocities (Table 5) allow us to calculate heliocentric velocities (U, V, W) from the algorithm of Johnson and Soderblom [32]. These five members seem to be giant

Table 5. For five likely members with Gaia DR2 radial velocity data (V_{rad}) km s^{-1}) (column 8), Gaia DR2 proper motion components $mas\ yr^{-1}$ (columns 6–7), and parallaxes (mas) (column 9). Their equatorial coordinates (J2000) (columns 2–3) and V and $(B-V)$ (columns 4–5). Probability membership value (last column).

STAR-ID	RA	DEC	V	$(B-V)$	$\mu_\alpha \pm \sigma_{\mu\alpha}$	$\mu_\delta \pm \sigma_{\mu\delta}$	$V_{rad} \pm \sigma_V$	$\varpi \pm \sigma_\varpi$	P(%)
508	30.3497	75.5020	12.932	2.226	2.716 ± 0.064	0.397 ± 0.066	-28.05 ± 3.20	0.239 ± 0.040	99.77
862	30.1545	75.4700	13.936	2.165	2.476 ± 0.048	0.420 ± 0.051	-26.40 ± 0.78	0.257 ± 0.032	99.66
737	30.2315	75.4944	14.520	1.918	2.643 ± 0.040	0.484 ± 0.039	-28.55 ± 0.84	0.302 ± 0.024	99.73
299	30.5162	75.4812	14.615	1.956	2.483 ± 0.041	0.500 ± 0.041	-30.88 ± 0.92	0.273 ± 0.025	99.67
674	30.2739	75.4492	14.963	1.707	2.588 ± 0.036	0.261 ± 0.038	-31.57 ± 3.86	0.235 ± 0.023	99.67

candidates according to their V and $(B-V)$ values (left panel of Figure 8). The calculated U, V, and W velocities have been transformed to the components U', V', and W' by correcting for the solar motion $(U,V,W)_\odot = (+11.10, +12.24, +7.25)$ km s^{-1} with respect to the local standard of rest (LSR) [33]. We adopt $R_\odot = 8.2 \pm 0.1$ kpc [34] and $V_{LSR} = 239\,\mathrm{km\,s^{-1}}$ [35]. We adopt the right-hand system for the estimations. Their estimated heliocentric Cartesian distances (x', y', z') (kpc) and LRS-velocity components (U', V', W') have been transformed to Galactic Rest of Frame (GSR), i.e. (x, y, z) (kpc) and (V_x, V_y, V_z), via the equations given by Kepley et al. [36]. The Galactocentric velocity component (V_Φ) (km s^{-1}) (or azimuthal velocity) in a cylindrical frame is estimated via $V_\Phi = \frac{xV_y - yV_x}{R}$. $V_\Phi < 0$ means prograde. Thus, the obtained kinematic parameters (U, V, W, V_Φ) km s^{-1} are listed in columns 2–5 of Table 6.

By utilizing the "MWPotential2014" code in the galpy-code library [1] written by Bovy [37], peri- and apo-Galactic distances ($R_{\rm min}$, $R_{\rm max}$) (kpc) and the maximum height distance (z_{max}) (kpc) have been obtained. The orbital eccentricity (ecc) is estimated via the relation $e = (R_{\rm max} - R_{\rm min})/(R_{\rm max} + R_{\rm min})$. Mean orbital radius ($R_m$) (kpc) is given as the mean of $R_{\rm min}$ and $R_{\rm max}$ distances. Each member's orbit has been integrated for 2.8 Gyr (Table 4) within the Galactic potential. The Galactic potential is a sum of the Galactic components, as given in the paper of Bovy [37].

Table 6. For five probable members of Be 8, kinematics (U, V, W, V_Φ) km s^{-1} (columns 2–5) and orbital parameters (R_{max}, R_{min}, R_m, z_{max} (kpc)) and ecc (columns 6–10). Their orbital angular momentum values (J_z and $J_\perp$) (kpc km s^{-1}) (columns 11–12).

STAR-ID	U	V	W	V_Φ	R_{max}	R_{min}	R_m	z_{max}	ecc	J_z	$J_\perp$
508	-19.77	-55.89	15.36	-184.42	12.44	6.69	9.56	1.27	0.30	-2056.63	259.33
862	-14.94	-49.42	13.32	-192.93	12.12	7.09	9.60	1.15	0.26	-2106.96	242.69
737	-10.64	-48.43	11.61	-196.75	11.32	7.10	9.21	0.97	0.23	-2060.68	218.84
299	-9.91	-51.27	12.69	-193.21	11.66	7.07	9.37	1.07	0.24	-2076.34	235.59
674	-17.44	-57.54	11.64	-183.29	12.40	6.68	9.54	1.21	0.30	-2054.53	233.05

The orbital angular momentum components J_x, J_y, J_z, and $J_\perp$ (kpc km s^{-1}) for five members are calculated from the equations of Kepley et al. [36]. These orbital and angular momentum parameters (J_z, $J_\perp$)

[1] http://github.com/jobovy/galpy [accessed 20 May 2019].

are given in columns 6–12 of Table 6. The total angular momentum J$_\perp$ is defined as $J_\perp = (J_x^2 + J_y^2)^{1/2}$. For example, the right-handed J$_z$ value of a star near the Sun is -1960 kpc km s^{-1} from the solar values of R$_\odot$ and V_{LSR}.

The vertical heliocentric velocities of W = [12, 15] km s^{-1} and azimuthal velocities, $V_\Phi = [-183, -197]$ km s^{-1} of these five likely members indicate that they have typical Galactic disc velocities. They reside in the outer Galactic disc, $R_m > 8.5$ kpc with the circular orbits, ecc = [0.23, 0.30]. Their Galactic heights reach $z_{max} = 1.27$ kpc . According to Figure 13 of Carney et al. [38], thin and thick disc stars have orbital eccentricities with $ecc <$ [0.25, 0.30] (circular orbits) and $0.30 < ecc < 0.45$ (elliptical). In this sense their orbital parameters reflect the properties of the Galactic thin disc. This is also consistent with what is expected of its metal content, [M/H] = –0.27.

The Galactic orbits of five probable members of Be 8 are presented in Figures 11a and 11b. Five likely members with the circular orbits move from ∼12 kpc to ∼7 kpc on x – y (kpc) (panel a). On z – R (kpc) (panel b), they reach z ∼1.3 kpc for the range of $6 < R < 12$ kpc. Here R means the Galactocentric distance. The angular momentums (J$_\perp$, J$_z$) of these members fall in the range of $220 < J_\perp < 262$ kpc km s^{-1} for $-2107 \leq J_z \leq -2054$ kpc km s^{-1}. Their kinematics, dynamical, and angular momentum values imply the indicators of the Galactic thin disc population, according to Figure 11 of Kepley et al. [36].

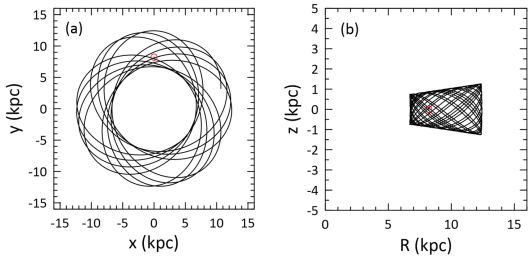

Figure 11. The orbits of five probable members of Be 8 on x – y (kpc) (panel a) and z – R (kpc) (panel b). Large circle denotes the position of the Sun, $(z_\odot,\ R_\odot) = (0,\ 8.2\ kpc)$.

8. Discussion and conclusions

For the cluster members of Be 8, the reddenings E$(B-V) = 0.69 \pm 0.03$ and E$(V-I) = 0.87 \pm 0.10$ have been obtained from V - $(B-V)$ and V - $(V-I)$ diagrams (Figure 8). These values are in good concordance with the ones of E$(B-V) = 0.75$ and E$(V-I) = 0.88$ given by Hasegawa et al. [1]. Our E$(B-V)$ value is larger than the value of 0.41 given by Bukowiecki et al. [2] for 2MASS JHK$_s$ photometry.

Our distance modulus and distance from V - $(B-V)$ are (V_0 - M_V, d(pc)) = (12.66 ± 0.19, 3410 ± 300 pc), which are in good agreement with the value of (12.49, 3148 pc) of Hasegawa et al. [1]. Our value is somewhat smaller than the value of (13.34, 3960 pc) of Bukowiecki et al. [2]. Our distance modulus/distance (pc) and age (Gyr) from $G-(G_{BP}$ - $G_{RP})$ are quite compatible with the ones of the color indices, $(B-V)$, $(V-I)$, and $(R-I)$ (Table 4). The median Gaia DR2 parallax from 43 likely members ($\sigma_\varpi/\varpi < 0.20$) gives us $\varpi = 0.272 \pm 0.060$ mas, which corresponds to d = 3676 ± 810 pc. This distance is in good concordance with the photometric distances (3410–3620 pc) within the uncertainties (Table 4). A global systematic offset of Gaia DR2 parallaxes is $\Delta\varpi = -0.029$ mas in terms of an inertial reference frame, derived by Lindegren et al. [4]. Recent values for the zero point shift of the parallax have been found as $\Delta\varpi = -0.045 \pm 0.009$ mas [39],

$\Delta\varpi = -0.053 \pm 0.003$ mas [40], and $\Delta\varpi = -0.046 \pm 0.013$ mas [41], respectively. A correction of 0.005 mas to the median value of our median parallax gives a closer distance with a difference of 66 pc for Be 8.

The age of Be 8 is 2.80 ± 0.20 Gyr and this is younger than the 3.16 Gyr of Hasegawa et al. [1] and Bukowiecki et al. [2]. Its MAI age (A = 2.94 Gyr) is concordant with its isochrone age. Discrepancies of the distance moduli, distances, and ages as compared to the literature stem from the usage of different heavy element abundances, isochrones, reddenings, and photometries such as 2MASS JHK$_s$, as mentioned by Moitinho [42].

Two BS candidates reside in the core radius of 1.8′ of Be 8 (Figure 10). BS stars potentially locate in the inner regions of stellar clusters [43]. According to Ferraro [44], their ways of formation are explained: mass transfer in binary systems [45] due to the merging of the two stars and stellar collisions [46].

It is surprising to find Be 8 with $[M/H] = -0.27$ (close to solar metallicity) at such a large Galactic radius (R = 10.57 kpc). However, the orbits in Figures 11a and 11b show that the cluster passed a part of its time at Galactocentric radius $R = 6 - 7$ kpc, and then possibly it was born at that radius, which would explain the metallicity. According to Figures 3 and 4 ($[M/H]$ versus R (kpc)) of Lepine et al. [47], Be 8 with $[M/H] = -0.27$ and R = 10.57 kpc resides in a region of R > 9 kpc (co-rotation gap at 9 kpc). In the sense it may have been originating from a different galactic radius or different star formation region [47].

Acknowledgments

We wish to thank the staff of the Sierra Nevada Observatory, Granada, Spain. The second author acknowledges the financial support from the UNAM under DGAPA grant PAPIIT IN100918. We thank J. Lepine for his valuable comments. This paper has made use of results from the European Space Agency (ESA) space mission Gaia, the data from which were processed by the Gaia Data Processing and Analysis Consortium (DPAC). Funding for the DPAC has been provided by national institutions, in particular the institutions participating in the Gaia Multilateral Agreement. The website of the Gaia mission is http://www.cosmos.esa.int/gaia.

References

[1] Hasegawa T, Malasan HL, Hideyo KH, Obayashi H, Kurabayashi T et al. New photometric data of old open clusters in the Anti-Galactic Center Region. Publications of the Astronomical Society of Japan 2004; 56: 295. doi: 10.1093/pasj/56.2.295

[2] Bukowiecki L, Maciejewski G, Konorski P, Strobel A. Open clusters in 2MASS photometry. I. Structural and basic astrophysical parameters. Acta Astronomica 2011; 61: 231-246.

[3] Mermilliod JC. The database for stars in open clusters. II. A progress report on the introduction of new data. Bulletin d'Information du Centre de Donnees Stellaires 1992; 40: 115.

[4] Lindegren L, Hernandez J, Bombrun A, Klioner S, Bastian U et al. Gaia Data Release 2. The astrometric solution. Astronomy and Astrophysics 2018; 616: A2. doi: 10.1051/0004-6361/201832727

[5] Brown AGA, Vallenari A, Prusti T, de Bruijne JHJ, Babusiaux C et al. Gaia Data Release 2. Summary of the contents and survey properties. Astronomy and Astrophysics 2018; 616: A1. doi: 10.1051/0004-6361/201833051

[6] Balaguer-Nunez L, Tian KP, Zhao JL. Determination of proper motions and membership of the open clusters NGC 1817 and NGC 1807. Astronomy and Astrophysics, Supplement Series 1998; 133: 387. doi: 10.1051/aas:1998324

[7] Sariya DP, Yadav RKS, Bellini A. Proper motions and membership probabilities of stars in the region of globular cluster NGC 6809. Astronomy and Astrophysics 2012; 543: 87. doi: 10.1051/0004-6361/201219306

[8] Dias WS, Monteiro H, Lepine JRD, Prates R, Gneiding CD et al. Astrometric and photometric study of Dias 4, Dias 6, and other five open clusters using ground-based and Gaia DR2 data. Monthly Notices of the Royal Astronomical Society 2018; 481: 3887. doi: 10.1093/mnras/sty2341

[9] Roeser S, Demleitner M, Schilbach E. The PPMXL Catalog of Positions and proper motions on the ICRS. Combining USNO-B1.0 and the Two Micron All Sky Survey (2MASS). The Astronomical Journal 2010; 139: 2440-2447. doi: 10.1088/0004-6256/139/6/2440

[10] Skrutskie MF, Cutri R, Stiening R, Weinberg MD, Schneider SE et al. The Two Micron All Sky Survey (2MASS). The Astronomical Journal 2006; 131: 1163-1183 doi: 10.1086/498708

[11] Cantat-Gaudin T, Jordi C, Vallenari A, Bragaglia A, Balaguer-Nunez L et al. A Gaia DR2 view of the Open Cluster population in the Milky Way. Astronomy and Astrophysics 2018; 618: 93. doi: 10.1051/0004-6361/201833476

[12] Zacharias N, Finch CT, Girard TM, Henden A, Bartlett JL et al. The Fourth US Naval Observatory CCD Astrograph Catalog (UCAC4). The Astronomical Journal 2013; 145: 44. doi: 10.1088/0004-6256/145/2/44

[13] Landolt AU. UBVRI photometric standard stars around the Celestial Equator: updates and additions. The Astronomical Journal 2009; 137: 4186-4269. doi: 10.1088/0004-6256/137/5/4186

[14] van Dokkum PG. Cosmic-ray rejection by Laplacian edge detection. Publications of the Astronomical Society of the Pacific 2001; 113: 1420-1427. doi: 10.1086/323894

[15] Cutri RM, Wright EL, Conrow T, Fowler JW, Eisenhardt PRM et al. VizieR Online Data Catalog: AllWISE Data Release (Cutri+ 2013). VizieR On-line Data Catalog: II/328. 2013; 2328: 0C.

[16] Akkaya İ, Schuster WJ, Michel R, Chavarría KC, Moitinho A et al. CCD UBVRI photometry of the Galactic open clusters: Be 89, Ru 135, and Be 10. The Revista Mexicana de Astronomia y Astrofisica 2010; 46: 385.

[17] Akkaya Oralhan I, Karataş Y, Schuster WJ, Michel R, Chavarría KC. CCD UBV(RI)(C) photometry of twenty open clusters. New Astronomy 2015; 34: 195. doi: 10.1016/j.newast.2014.06.011

[18] Bonatto CH, Bica E. Old open clusters in the inner Galaxy: FSR1744, FSR89 and FSR31. Astronomy and Astrophysics 2007; 473: 445. doi: 10.1051/0004-6361:20077675

[19] King IR. The structure of star clusters. III. Some simple dynamical models. The Astronomical Journal 1966; 71: 64. doi: 10.1086/109857

[20] Pedregosa F, Varoquaux G, Gramfort A, Michel V, Thirion B et al. Scikit-learn: Machine learning in Python. Journal of Machine Learning Research 2011; 12: 2825-2830.

[21] Wu ZY, Tian KP, Balaguer-Nunez L, Jordi C, Zhao JL et al. Determination of proper motions and membership of the open star cluster NGC 2548. Astronomy and Astrophysics 2002; 381: 464. doi: 10.1051/0004-6361:20011474

[22] Schmidt-Kaler T. Physical parameters of the stars. In: Schaifers K, Voigt HH (editors). Numerical Data and Functional Relationships in Science and Technology, New Series, Group VI, Vol. 2b. Berlin, Germany: Springer Verlag, 1982. p. 14.

[23] Karataş Y, Schuster WJ. Metallicity and absolute magnitude calibrations for UBV photometry. Monthly Notices of the Royal Astronomical Society 2006; 371: 1793. doi: 10.1111/j.1365-2966.2006.10800.x

[24] Bressan A, Marigo P, Girardi L, Salasnich B, Dal Cero C et al. PARSEC: stellar tracks and isochrones with the PAdova and TRieste Stellar Evolution Code. Monthly Notices of the Royal Astronomical Society 2012; 427: 127. doi: 10.1111/j.1365-2966.2012.21948.x

[25] Güneş O, Karataş Y, Bonatto C. A dynamical evolution study of 40 2MASS open clusters. Astronomische Nachrichten 2017; 338: 464. doi: 10.1002/asna.201712978

[26] Dean JF, Warren PR, Cousins AWJ. Reddenings of Cepheids using BVI photometry. Monthly Notices of the Royal Astronomical Society 1978; 183: 569. doi: 10.1093/mnras/183.4.569

[27] Mathis J. Interstellar dust and extinction. Annual Review of Astronomy and Astrophysics 1990; 28: 37. doi: 10.1146/annurev.aa.28.090190.000345

[28] Straizys V. Multicolor Stellar Photometry. Astronomy and Astrophysics Series, Vol. 15. Tucson, AZ, USA: Pachart Pub. House, 1995.

[29] Bragaglia A, Fu X, Mucciarelli A, Andreuzzi G, Donati P. The chemical composition of the oldest nearby open cluster Ruprecht 147. Astronomy and Astrophysics 2018; 619: A176. doi: 10.1051/0004-6361/201833888

[30] Phelps RL, Janes KA, Montgomery KA. Development of the Galactic disk: a search for the oldest open cluster. The Astronomical Journal 1994; 107: 1079. doi: 10.1086/116920

[31] Salaris M, Weiss A, Percival SM. The age of the oldest open clusters. Astronomy and Astrophysics 2004; 414: 163. doi: 10.1051/0004-6361:20031578

[32] Johnson DRH, Soderblom DR. Calculating galactic space velocities and their uncertainties, with an application to the Ursa Major group. The Astronomical Journal 1987; 93: 864. doi: 10.1086/114370

[33] Schönrich R, Binney J, Dehnen W. Local kinematics and the local standard of rest. Monthly Notices of the Royal Astronomical Society 2010; 403: 1829. doi: 10.1111/j.1365-2966.2010.16253.x

[34] Bland-Hawthorn J, Gerhard O. The galaxy in context: structural, kinematic and integrated properties. Annual Review of Astronomy and Astrophysics 2016; 54: 529. doi: 10.1146/annurev-astro-081915-023441

[35] Brunthaler A, Reid MJ, Menten KM, Zheng XW, Bartkiewicz A et al. The Bar and Spiral Structure Legacy (BeSSeL) survey: mapping the Milky Way with VLBI astrometry. Astronomische Nachrichten 2011; 332 (5): 461. doi: 10.1002/asna.201111560

[36] Kepley A, Morrison HL, Helmi A, Kinman TD, van Duyne J et al. Halo star streams in the solar neighborhood. The Astronomical Journal 2007; 134: 1579. doi: 10.1086/521429

[37] Bovy J. galpy: A python library for galactic dynamics. Astronomy and Astrophysics, Supplement Series 2015; 216: 29. doi: 10.1088/0067-0049/216/2/29

[38] Carney BW, Laird JB, Latham DW, Aguilar LA. A survey of proper motion stars. XIII. The Halo population. The Astronomical Journal 1996; 112: 668. doi: 10.1086/118042

[39] Yalyalieva LN, Chemel AA, Glushkova EV, Dambis AK, Klinichev AD. A comprehensive study of 94 open clusters based on the data from IPHAS, GAIA DR2, and other sky surveys. Astrophysical Bulletin 2018; 73: 335. doi: 10.1134/S1990341318030070

[40] Zinn JC, Pinsonneault MH, Huber D, Stello D. Confirmation of the Gaia DR2 parallax zero-point offset using asteroseismology and spectroscopy in the Kepler field. The Astronomical Journal 2018; 878: 1538-4357. doi: 10.3847/1538-4357/ab1f66

[41] Riess AG, Casertano S, Yuan W, Macri L, Bucciarelli B et al. Milky Way Cepheid standards for measuring cosmic distances and application to Gaia DR2: implications for the Hubble constant. The Astronomical Journal 2018; 861: 126. doi: 10.3847/1538-4357/aac82e

[42] Moitinho A. Star clusters: basic galactic building blocks. In: Proceedings of IAU Symposium No. 266; 2010.

[43] Carney B. Star Clusters, Saas-Fee Advanced Course 28, Lecture Notes 1998, Swiss Society for Astrophysics and Astronomy. Berlin, Germany: Springer-Verlag, 2001.

[44] Ferraro FR. IAUS-Star clusters and black holes in galaxies across cosmic time. In: Proceedings of the International Astronomical Union, IAU Symposium; 2016. pp. 171-180.

[45] McCrea WH. Extended main-sequence of some stellar clusters. Monthly Notices of the Royal Astronomical Society 1964; 128: 147. doi: 10.1093/mnras/128.2.147

[46] Hills J, Day C. Stellar collisions in globular clusters. Astrophysical Letters 1976; 17: L87.

[47] Lepine JRD, Cruz P Scarano S, Barros DA, Dias WS et al. Overlapping abundance gradients and azimuthal gradients related to the spiral structure of the Galaxy. Monthly Notices of the Royal Astronomical Society 2011; 417: 698. doi: 10.1111/j.1365-2966.2011.19314.x